Advances in Nano Research, *Vol. 7 No. 4 (2019) 233-240*
DOI: https://doi.org/10.12989/anr.2019.7.4.233

Apoptosis and inhibition of human epithelial cancer cells by ZnO nanoparticles synthesized using plant extract

Vaibhav Koutu, Shweta Rajawat*, Lokesh Shastri and M.M. Malik

Nanotechnology Research Laboratory, Department of Physics and Nanoscience & Engineering, Maulana Azad National Institute of Technology, Bhopal, MP, India

(*Received April 23, 2018, Revised May 1, 2019, Accepted June 19, 2019*)

Abstract. The present research work reports in-*vitro* anti-cancer activity of biologically synthesized ZnO nanoparticles (ZnO NPs) against human carcinoma cells viz SCC-40, SK-MEL-2 and SCC-29B using Sulforhodamine-B (SRB) Assay. ZnO NPs were synthesized by a unique and novel biological route using Temperature-gradient phenomenon where the extract of combination of *Catharanthus roseus* (L.) G. Don (C. *roseus*), *Azadirachta indica* (A. *indica*), *Ficus religiosa* (F. *religiosa*) and NaOH solution were used as synthesis medium. The morphology of the ZnO NPs was characterized by Transmission Electron Microscopy (TEM). TEM images reveal that particle size of the samples reduces from 76 nm to 53 nm with the increase in reaction temperature and 68 nm to 38 nm with the increase in molar concentration of NaOH respectively. XRD study confirms the presence of elements and reduction in crystallite size with increase in reaction temperature and NaOH concentration. The diffraction peaks show broadening and a slight shift towards lower Bragg angle (2θ) which represents the reduction in crystallite size as well as presence of uniform strain. The FTIR spectra of the extract show transmittance peak fingerprint of Zn-O bond and presence of bioactive molecules These NPs exhibit inhibition greater than 50% for SCC-40, SK-MEL-2 and SCC-29B cell lines and more than 50% cell kill for SCC-29B cells at concentrations < 80 μg/ml. Nanoparticles with smallest size have shown better anti-cancer activity and peculiar cell-selectivity. The combination of extracts of these plants with ZnO NPs can be used in targeted drug delivery as an effective anti-cancer agent, a potential application in cancer treatment.

Keywords: C. roseus; A. indica; F. religiose; ZnO; Apoptosis

1. Introduction

Zinc oxide nanoparticles (ZnO NPs) have clutched the attention of scientists because of their excellent optical properties and wide utilization in biomedical applications (Rasmussen *et al*. 2010). Zinc oxide also finds application in various branches of industry, e.g., concrete production (Xiao *et al*. 2014), photocatalysis (Wang *et al*. 2014) electronics (Kołodziejczak-Radzimska and Jesionowski 2014), dual-functional gas sensing (Tian *et al*. 2014, 2018), hydrogen peroxide sensing (Tian *et al*. 2017) etc. It has been vindicated that at lower dimensions the physical, chemical, electrical, morphological, magnetic, optical and transport properties of the materials changes drastically, however the most significant enhancement is observed in their biomedical properties. At nano scale, the surface to volume ratio increases many folds which enable the NPs to interact with the cell biomolecules. NPs penetrate inside the cell structures and cause significant alterations in the metabolic activities of the cells (Rasmussen *et al*. 2010, Bisht and Rayamajhi 2016, Nam *et al*. 2016). These outstanding properties and better adherence to the cell molecules classifies NPs as potential candidates in the field of diagnostics, drug delivery, imaging and therapeutic devices (Nam *et al*. 2016). Amongst various biomedical applications, nanomedicines with better control over the size and target-selectivity have gained special attention to cure and possibly eradicate many diseases (Bisht and Rayamajhi 2016). One of the vastly explored applications of nanomedicines is the development of anti-cancer NPs with maximum cancer-apoptosis and minimal toxicity to the normal cells.

Cancer is a state of uncontrolled cell differentiation and cell growth. It has been conventionally treated using chemotherapy, surgery and radiation over many decades (Bisht and Rayamajhi 2016, Dhamodaran and Kavitha 2015). Major drawback of conventional therapies for cancer treatment is damage to the normal healthy cells which led to the development of advanced anti-cancer nanomedicines with better targeted drug-delivery and cell-selectivity. One of the potential materials used in this field are metal-oxide NMs, which by enhanced surface electrochemical properties and cell selectivity, have shown significant advances over the noble metallic NPs (Bisht and Rayamajhi 2016). Various researchers have explored and reported the potential anti-cancer activities of several metal-oxide nanomaterials (NMs) like iron-oxide NMs (Gurunathan *et al*. 2015), cerium-oxide NMs (Bisht and Rayamajhi 2016), titanium-oxide NMs (Garcia-Contreras *et al*. 2014), copper-oxide NMs (Fiorillo *et al*. 2015, Sankar *et al*. 2014, Nagajyothi *et al*. 2017), Zinc-oxide NMs (Arakelova *et al*. 2014, Krishna *et al*. 2016), and graphene-oxide flakes

*Corresponding author, Post-Doctoral Fellow,
E-mail: srajawat73@gmail.com

ISSN: 2287-237X (Print), 2287-2388 (Online)

(Fiorillo *et al*. 2015). Amongst them, ZnO NPs show promising efficiency and application in cancer therapy because of their high biocompatibility, cell-selectivity, easy synthesis, enhanced cytotoxicity and high potency towards cancer cells. Recent studies have shifted the focus on the use of plant extracts for the reduction of precursors and synthesis of NPs (Namvar *et al*. 2016) as these extract-synthesized NMs are eco-friendly, non- toxic, have high adherence and especially can be tuned to specific target-cell for appliance. Wide varieties of plants have been used for the synthesis of various inorganic NPs (Mittal *et al*. 2013), amongst them Catharanthus *roseus* (L.) G.Don (Madagascar periwinkle) (*C. roseus*) is one of the most studied plant for anti-cancer activities due to high cytotoxicity (DerMarderosian and Beutler 2012). *C. roseus*, belonging to the family Apocynaceae, produces more than 100 monoterpenoidindole alkaloids (MIAs) including two commercially important cytotoxic dimeric alkaloids - vincaleukoblastine (vinblastine) and leurocristine (vincristine) which are used in cancer therapy (Magnotta *et al*. 2006, Lucas *et al*. 2010).

In the present study, authors have designed a novel method, according to the best of authors' knowledge, for the synthesis of ZnO NPs using the shoot extract of the mixture of A. *indica* and F. *religiosa* and pedicels of *C. roseus* as reaction medium (Koutu *et al*. 2017). *C. roseus* leaves were selected as they exhibit cytotoxicity and *A. indica* and *F. religiosa* were used to enhance the biocompatibility of the samples. Anti-cancer activity of the as-prepared ZnO was investigated against human epidermal cancer cells viz. SK-MEL-2 (Skin Melanoma), SCC-40 (Oral Squamous) and SCC-29B (Oral Squamous).

2. Methodology

2.1 Initial materials

20 grams fresh shoots of each A. *indica* and F. *religiosa*, 20 grams pedicels of C. *roseus*.

2.2 Precursors

Zinc acetate dihydrate (Zn(CH3COO)2.2H2O) and Sodium hydroxide (NaOH) of 99.95% purity were purchased from Sigma-Aldrich and used as-procured,Ethanol (99.9% pure - Merck Millipore), Double-distilled water (prepared in laboratory).

2.3 Plant extract preparation

Plant extract was prepared by reflux-boiling of the leaf mixture for 2 hours.

2.4 Synthesis of ZnO nanoparticles using extract

1M of Zn(CH3COO)2.2H2O was added to 100 ml of extract (pre-heated at 80°C) in a sealed flask and stirred at 700 rpm. 100 ml of equimolar Sodium hydroxide (dissolved in plant extract, at room temperature) was added to the pre-heated zinc solution and the mixture was stirred for 1 hour at 80°C. It was then refluxed at 80°C for 1 hour. The final mixture was precipitated at room temperature and washed three times with methanol. The final precipitate was then vacuum-dried at room temperature to obtain the end product (Zinc oxide). Same procedure was followed to prepare Zinc oxide at different reaction temperatures (90°C and 100°C) keeping Zn(CH3COO)2.2H2O: NaOH molar ratio fixed at 1:1 and these samples are categorized as A1, A2 and A3. Further, another set of ZnO samples were prepared by varying Zn(CH3COO)2.2H2O: NaOH molar ratio as 1:1, 1:2 and 1:3 using similar method at 90°C. These samples are categorized as B1, B2 and B3.

2.5 Procedure for Sulforhodamine B (SRB) assay for anti-cancer activity

(1) The cell lines were grown in RPMI 1640 medium containing 10% fetal bovine serum and 2 mM L-glutamine. For present screening experiment, cells were inoculated into 96 well microtiter plates in 100 µL at plating densities as shown in the study details above, depending on the doubling time of individual cell lines. After cell inoculation, the microtiter plates were incubated at 37°C, 5% CO2, 95% air and 100% relative humidity for 24 hours prior to addition of experimental drugs.

(2) Experimental drugs were initially solubilized in dimethyl sulfoxide at 100 mg/ml and diluted to 1 mg/ml using water and stored frozen prior to use. At the time of drug addition, an aliquot of frozen concentrate (1 mg/ml) was thawed and diluted to 100 μg/ml, 200 μg/ml, 400 μg/ml and 800 μg/ml with complete medium containing test article. Aliquots of 10 μl of these different drug dilutions were added to the appropriate microtiter wells already containing 90 μl of medium, resulting in the required final drug concentrations i.e., 10 μg/ml, 20 μg/ml, 40 μg/ml, 80 μg/ml.

(3) After compound addition, plates were incubated at standard conditions for 48 hours and assay was terminated by the addition of cold TCA. Cells were fixed in situ by the gentle addition of 50 μl of cold 30% (w/v) TCA (final concentration, 10% TCA) and incubated for 60 minutes at 4°C. The supernatant was discarded; the plates were washed five times with tap water and air dried. Sulforhodamine B (SRB) solution (50 μl) at 0.4% (w/v) in 1% acetic acid was added to each of the wells, and plates were incubated for 20 minutes at room temperature. After staining, unbound dye was recovered and the residual dye was removed by washing five times with 1% acetic acid. The plates were air dried. Bound stain was subsequently eluted with 10 mM trizma base, and the absorbance was read on a plate reader at a wavelength of 540 nm with 690 nm reference wavelength.

(4) Percent growth was calculated on a plate-by-plate basis for test wells relative to control wells. Percent Growth was expressed as the ratio of average absorbance of the test well to the average absorbance of the control wells * 100.

(5) Using the six absorbance measurements [time zero

Table 1 Details of sample preparation

S. No.	Sample	Precursor Concentration (Zinc Acetate)	(NaOH)	Molar Ratio	Reaction Temperature	Heating time
1.	A1	0.1M	0.1M	1:1	80°C	2 hrs
2.	A2	0.1M	0.1M	1:1	90°C	2 hrs
3.	A3	0.1M	0.1M	1:1	100°C	2 hrs
4.	B1	0.1M	0.1M	1:1	90°C	2 hrs
5.	B2	0.1M	0.2M	1:2	90°C	2 hrs
6.	B3	0.1M	0.3M	1:3	90°C	2 hrs

(Tz), control growth (C), and test growth in the presence of drug at the four concentration levels (Ti)], the percentage growth was calculated at each of the drug concentration levels. Percentage growth inhibition was calculated as shown in Eq. (1)

$$\frac{\mathrm{Ti}}{c} * 100\% \quad (1)$$

The crystal structure and purity of the samples was characterized using X-ray diffractometer Rigaku MiniFlex II (1.54Å Cu-Kα radiation) in the range 20°-80° (2θ) at scan rate of 3°/minute. Particle size analysis and distribution was studied using 120 kV High-Resolution Transmission Electron Microscope (JEM-1400, Jeol, Japan). Optical transmittance and bond-analysis was studied by Bruker VERTEX-70 FTIR Spectrometer. In-vitro Anti-cancer activity of the samples was studied at Anti-Cancer Drug Screening Facility (ACDSF), Advanced Centre for Treatment, Research & Education in Cancer (ACTREC), Tata Memorial Centre, Navi Mumbai (India).

3. Results and discussion

3.1 X-ray Diffraction (*XRD*)

Fig. 1 shows X-ray diffraction patterns of the samples prepared using extract of combination of plants. All the peaks in the obtained patterns are well matched with the JCPDS file #80-0075 of the standard ZnO which can be indexed corresponding to the hexagonal reflection of the wurtzite ZnO. No characteristic peaks of the impurity phases were observed. The average crystallite sizes (d) of as- prepared samples was calculated using Scherrer's. (Ashrafi and Almamun 2011, Mote *et al*. 2016).

The diffraction peaks show broadening and a slight shift towards lower Bragg angle (2θ) which represents the reduction in crystallite size as well as presence of uniform strain (Ashrafi and Almamun 2011, Mote *et al*. 2016, Zak *et al*. 2011). This strain was calculated and explained using Williamson-Hall (W-H) method] which claims that the diffraction line broadening is due to strain (ε) effect and reduction in crystallite size. The crystallite size calculated from UDM plot and Scherrer's equation and the strain in the samples are tabulated in Table 2.

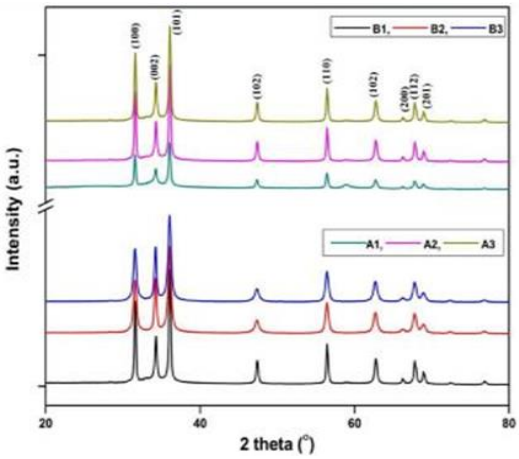

Fig. 1 XRD spectra of as-prepared ZnO samples

Table 2 Calculated values of average Crystallite size for the ZnO samples by UDM (W-H plot), Scherrer formula and HR-TEM, Strain and Surface Area

S. No.	Sample	Precursor Concentration (Zinc Acetate)	(NaOH)	Molar ratio	Reaction Temperature
A1	42 nm	31 nm	76 nm	3.86×10^{-3}	-
A2	39 nm	29 nm	64 nm	4.18×10^{-3}	13.12
A3	32 nm	24 nm	53 nm	4.75×10^{-3}	18.67
B1	25 nm	19 nm	68 nm	2.77×10^{-3}	13.01
B2	24 nm	18 nm	61 nm	3.21×10^{-3}	15.32
B3	22 nm	16 nm	38 nm	3.58×10^{-3}	-

From Table 2, it was observed that the crystallite size of the as-prepared ZnO samples is reducing with increase in the reaction temperature as well as increase in NaOH concentration, which is well supported by the corresponding increase in the value of strain (ε). A small variation is observed in the calculated values of the crystallite size obtained from both methods (W-H plot and Scherrer formula) which is because of the difference in averaging the particle size distribution (Koutu *et al*. 2017) These findings are in good agreement with the previous reported results which justify the reduction in crystallite size with increase in reaction temperature and NaOH concentration respectively (Koutu *et al*. 2016, 2017).

3.2 Morphological analysis

Morphology and average particle size of the samples was determined by High-Resolution Transmission Electron Microscope (HR-TEM). All the samples were characterized at 120 kV accelerating voltage. Fig. 2 represents the morphology and particle size distribution of the samples prepared at varying reaction temperature (Figs. 2(a)-(c)) and varying NaOH concentration (Figs. 2(d)-(f)) respectively.

From the HR-TEM images, it was clear that particles have spherical morphology and well-defined grain boundaries. Particles show slight agglomeration which can

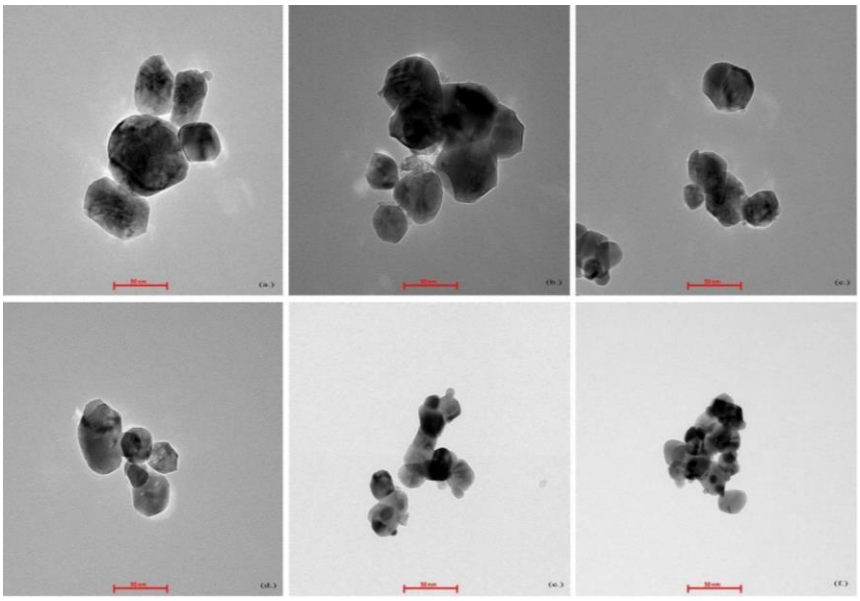

Fig. 2 Morphological Analysis of as-synthesized ZnO NPs:
(a) sample A1; (b) sample A2; (c) sample A3; (d) sample B1, (e) sample B2, and (f) sample B3

be attributed to the steps utilized during sample preparation for HR-TEM analysis. The average diameter of the NPs was calculated from the particle size distribution analysis and is listed in Table 2. The surface area of the samples was also calculated (Table 2) using AutosorbiQ BET instrument (Make: Quantachrome, USA).

From Table 2, it can be observed that particle size of the samples reduces from 76 nm (sample A1) to 53 nm (sample A3) and 68 nm (sample B1) to 38 nm (sample B3) with respect to increase in reaction temperature and NaOH concentration respectively. Also, the surface area increases simultaneously with reduction in particle size from 13.12 m^2/gm (A2) to 18.67 m^2/gm (A3) and 13.45 m^2/gm (B1) to 15.32 m^2/gm (B2). This increase in surface area will cause enhanced adherence with the cancer cells and the reduced dimension will allow the smaller nanoparticles to adsorb and penetrate the cell membrane causing high cancer cytotoxicity.

3.3 Fourier Transform Infrared Spectroscopy (*FTIR*)

The structural analysis of the as-synthesized samples was performed by FTIR transmission spectrum to ascertain the purity and nature of the material. Samples were characterized in the range 400-4000 cm^{-1} and the transmittance obtained was plotted as shown in Fig. 3. The region below 1000 cm^{-1} is known as the fingerprint region for all the metallic compounds (Fang *et al*. 2015). To study the presence of biomolecules in ZnO samples, a pure ZnO sample was prepared using the same method illustrated in (Koutu *et al*. 2017) using distilled water as reaction medium instead of plant extract.

FTIR spectra of NPs show the transmittance peak fingerprint of Zn-O bond around 551 cm^{-1}, which is the characteristic region for Zn-O (450-600 cm^{-1}) (Pourrahimi *et al*. 2015). Moreover, the FTIR of as- synthesized sample using plant extract (Fig. 3(b)), shows presence of bioactive molecules which may play role in the anti-cancer activity. The spectra show the spectral peaks corresponding to amides (1687 cm^{-1} – C = O stretch, 1757 cm^{-1} – C = N, 3408 cm^{-1} – N-H stretch), amines (1186 cm^{-1}, 1357 cm^{-1} – C-N stretch, 3408 cm^{-1} – N-H stretch (II)), alkyl halides (700 – 1000 cm^{-1}) and nitro groups (1516 cm^{-1} – N-O stretch).

One prominent difference in the spectra is observed in the alcoholic O-H (stretch, free) region (3500-3850 cm^{-1}) which shows occurrence of single broad strong peak for pure ZnO while 3 strong and sharp peaks are observed for as-synthesized ZnO. The presence of 3 peaks suggests availability of adsorbed free OH^- ions that can result in formation of ZnO^- and $ZnOH2^+$ molecules which may lead to an electrostatic interaction between ZnO NPs and cancerous cells, and finally cytotoxicity (Rasmussen *et al*. 2010, Bisht and Rayamajhi 2016). According to available reports (Rasmussen *et al*. 2010, Bisht and Rayamajhi 2016,

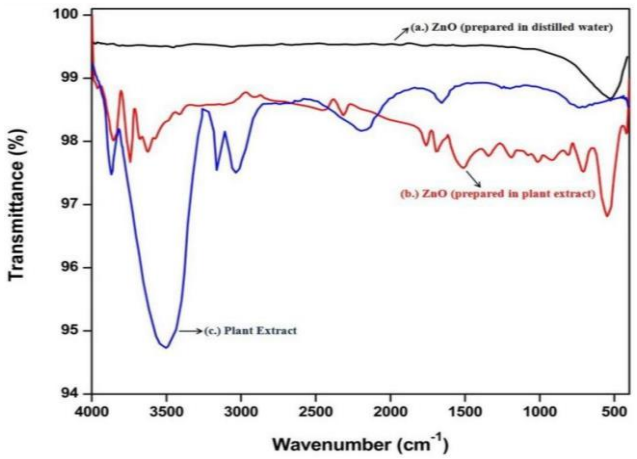

Fig. 3 FTIR spectra of ZnO NPs: (a) prepared in distilled water; (b) prepared in plant extract; (c) FTIR spectra of plant extract

Nam *et al*. 2016, Nagajyothi *et al*. 2017), the anti-cancer activity of ZnO is governed by the zinc-mediated protein activity mechanism followed by Reactive Oxygen Species (ROS) oxidative stress production, which in turn depends upon the free OH ions.

3.4 Anti-cancer activity analysis

In-*vitro*Anti-cancer activity of as-prepared ZnO NPs was tested against Human Oral Squamous Cell Carcinoma (SCC-40), Human Melanoma Cell Line (SK-MEL-2) and Human Oral Squamous Cell Carcinoma (SCC-29B) cell lines using Sulforhodamine B (SRB) assay. Cancer cell lines were grown in RPMI 1640 medium containing 10% fetal bovine serum and 2 mM L- glutamine (Figs. 5(a), 6(a) and 7(a)). The samples were initially dissolved in dimethyl sulphoxide and then experiment was performed at drug doses administered at different concentrations (10, 20, 40 and 80 μg/ml). The anti-cancer activity was analyzed at Anti-Cancer Drug Screening Facility (ACDSF), Advanced Centre for Treatment, Research & Education in Cancer (ACTREC), Tata Memorial Centre, Navi Mumbai (India).

Sample A3 showed comparatively much better cell killing efficiency against SCC-29B cancer cells as compared to SCC-40 and SK-MEL-2 cancer cells, suggesting a correlation in cell killing efficiency between particle size and cell type. From the growth curves (Fig. 4), it was inferred that sample B3 shows better inhibition for SCC-40 followed by A3 and A2; while sample A3 shows much enhanced growth inhibition for SK-MEL-2 cancer cells and remarkable cell kill for SCC-29B followed by A2, B2 and B3. The plots show that maximum growth inhibition was obtained at 80 μg/ml drug concentration while samples A2 and A3 show remarkable inhibition at 40 μg/ml drug concentration. Cell viability of SCC-40 cancer cells at 80 μg/ml drug concentration was 117% for A1, 24.4% for B3, 85.8% for B2, 57.8% for A2, and 30.8% for A3. Similarly, for SK-MEL-2 and SCC-29B cell lines, the cell viability

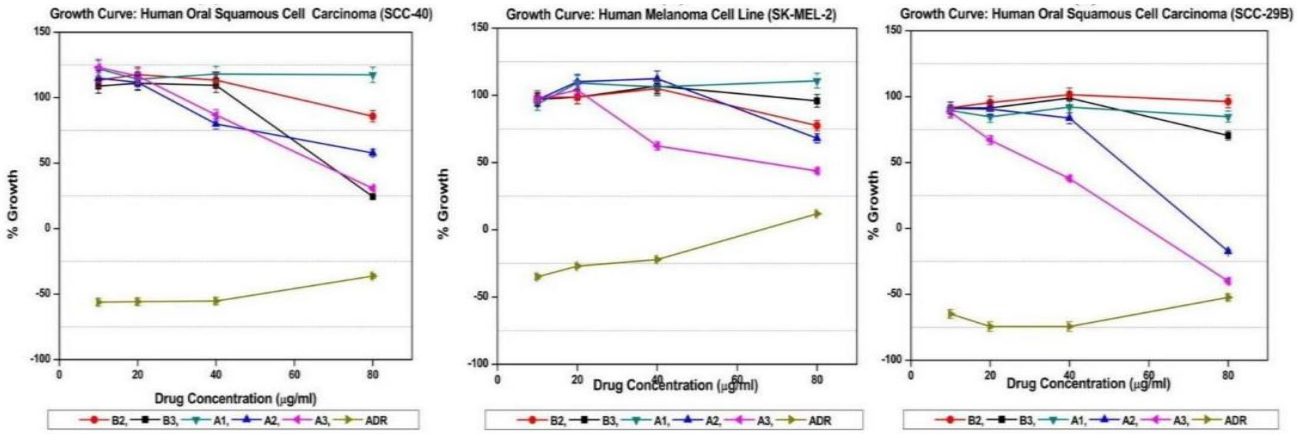

(a) (b) (c)

Fig. 4 Growth curves of ZnO NPS against human cancer cell lines: (a) Human Oral Squamous Cell Carcinoma (SCC-40); (b) Human Melanoma Cell Line (SK-MEL-2); (c) Human Oral Squamous Cell Carcinoma (SCC-29B). Data are expressed as a mean ± error (5%)

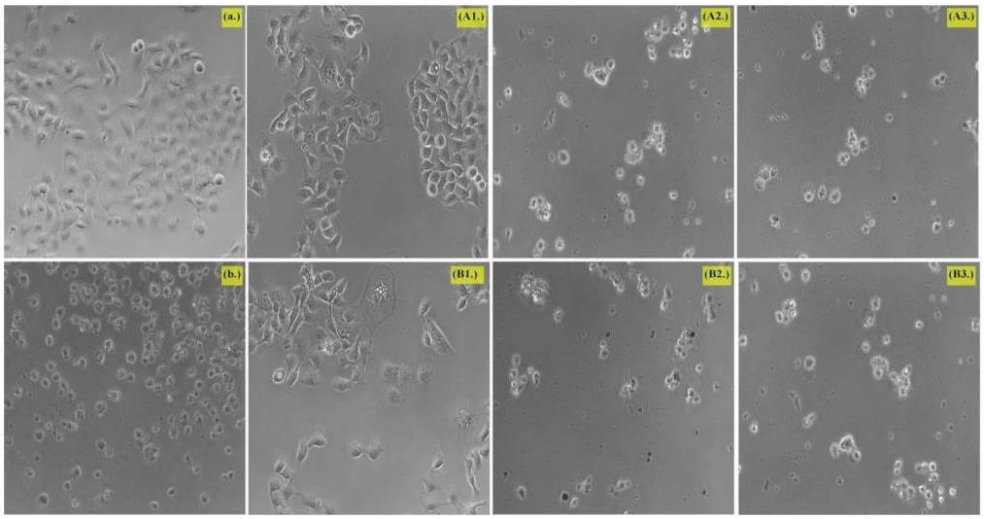

Fig. 5 In-vitro Anti-cancer activity of ZnO samples against SCC-40 cancer cell lines: (a) Control Growth; (b) Positive Control using ADR

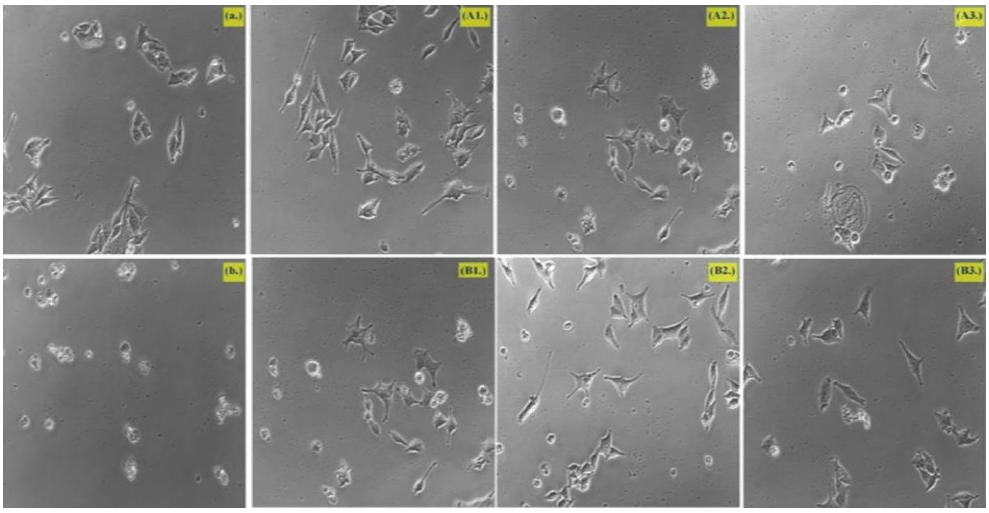

Fig. 6 In-vitro Anti-cancer activity of ZnO samples against SK-MEL-2 cancer cell lines: (a) Control Growth; (b) Positive Control using ADR

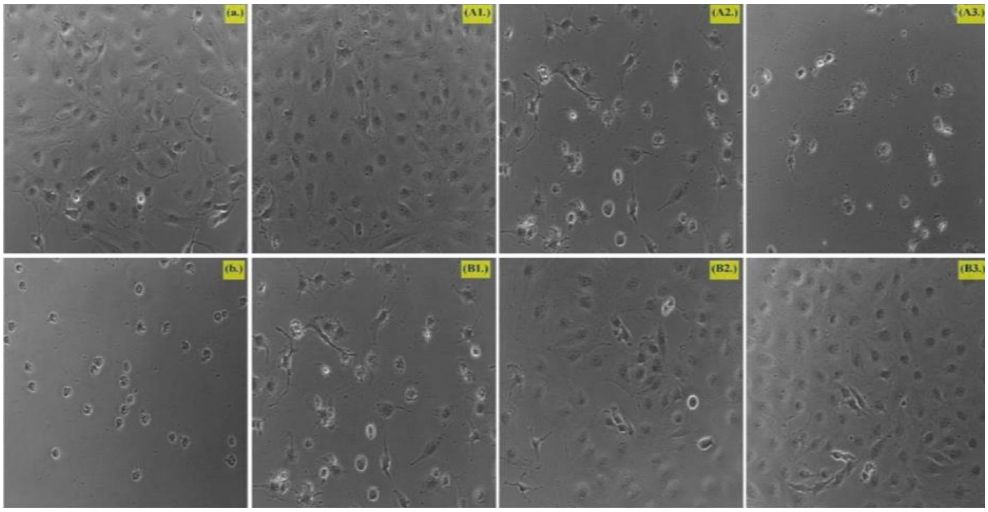

Fig. 7 In-vitro Anti-cancer activity of ZnO samples against SCC-29B cancer cell lines: (a) Control Growth; (b) Positive Control using ADR

was 110.1% for A1, 95.3% for B3, 77.5% for B2, 68.1% for A2 and B1, and 43.8% for A3; and 84.8% for A1, 70.5% for B3, 96.3% for B2, -17.3% for A2 and B1 (Total Growth Inhibition - TGI at 76.1 μg/ml) and -40% for A3 (TGI at 58.7 μg/ml) respectively. It can be inferred that sample B3 has maximum anti- cancer activity against SCC-40 cell lines; A3 has maximum activity against SCC-29B and SK-MEL-2 and also cytotoxicity against SCC-29B cell lines. The results suggest a relation between particles size and cancer cell type as all the cells have different anatomy and physiochemical properties and the NPs show selective adherence to a specific cancer cell type. It is also clear that at drug concentration of ~100 μg/ml, the samples will show total growth inhibition and also cytotoxicity for the corresponding cancer cell. From the in-*vitro* analysis, a comparative study of the cell samples shows a definitive cell death in control versus positive control (shown in (b) section of Figs. 5-7). Cells are rounded and cell death appears mainly due to apoptosis as cell peripheries are blabbed (Tang *et al*. 2014). Necrosis is also a possibility but blabbed peripheries are indicative of apoptosis (Tiong *et al*. 2013, El-Sayed *et al*. 2005). Samples B1, A2 and A3 seem to cause wide spread cell death. It is evident from images that samples B1, A2 and A3 do possess anti- cancer activity. Low cell density is symptomatic of their potency (Ahmad *et al*. 2015, Liu *et al*. 2017, Iwashita *et al*. 2000). Also, the effectiveness of these three samples B1, A2 and A3 looks comparable to one another. B2 and B3 also seem to cause cell death which is less pronounced in comparison to positive control or B1, A2 and A3samples. Moreover, there is shuttle difference between A1 and B3-induced cell death. Apparently, some cells retain their pointy shapes in the presence of drug A1 and B3. The images show a relation between the type of cancer cells and the size of NPs which was also observed from the growth curves (Fig. 4). The basic mechanism for the cytotoxicity of ZnO NPs is the intracellular release of dissolved Zn^{2+} ions followed by ROS induction (Nagajyothi *et al*. 2017) which in-turn

depends upon the electrostatic characteristic of ZnO NPs. It has been reported that the ROS generation ability (cytotoxicity) of ZnO NPs is related to the crystal defects in the NPs due to their nano size (Bisht and Rayamajhi 2016). From W-H analysis of the samples, it was clear that the particles show high values of stress which led to the development of defects in the crystal lattice of the samples. Rasmussen *et al*. (2016) have reported that ZnO NPs have neutral OH groups attached to their surface which determine their surface charge behavior. From the FTIR spectra (Fig. 3), it was clear that ZnO NPs have 3 free O-H (stretch) peaks which on reaction with cell fluids may lead to the formation of various Zn-based groups like $ZnOH2^{+}$, ZnOH, ZnO^{-} (Rasmussen *et al*. 2010) depending upon the pH and chemical composition of the extracellular fluid. This could trigger/initiate the particle-cell interaction between NPs and the cell surface which results in the kinetic and thermodynamic exchanges between the interfaces (Bisht and Rayamajhi 2016). This plays a vital role in the cellular uptake of NPs inside the cell which may cause NPs to directly interact with the cytoplasm proteins and cell organelles leading to cell toxicity and eventually cell death. Further, reports (Tiong *et al*. 2013) also suggest that there is a direct relation between the anti-cancer activity and size of the NPs. Since each cell has a characteristic morphology, surface pore size and physiochemical balance, it can be stated that for each cancer cell the optimum size of anti-cancer NPs can vary depending upon the cell physiology.

The optimum size of NPs for enhanced anti-cancer activity can be determined by the balance between the retention and clearance time duration of NP inside the cancer cell, because according to Tang *et al*. (2014), smaller NPs (< 2 nm) can traverse most cancer/tumor cells effectively and freely, but also they diffuse away the cells rapidly leading to minimal tumor retention time, while particles > 20 nm cannot clear the interstitial/lymphatic threshold (< 20 nm). From this phenomenon it can be inferred that optimum size of NPs for better anti-cancer activity is between 25-80 nm and from the particle size distribution of ZnO samples the particle size obtained were between 30-60 nm, which could also be possible cause of enhance anti-cancer activity of the samples.

4. Conclusions

ZnO samples prepared in extract of mixture of C. *roseus*, A. *indica and* F. *religiosa* via co-precipitation method using temperature gradient show good anti-cancer activity against human epithelial cancer cell lines. ZnO formation was confirmed by the FTIR analysis as well as X-ray diffraction analysis of the samples. Diffraction studies also showed the presence of significant compressive strain in the samples which had caused reduction in the crystallite size of the samples. This strain was developed due to the effect of temperature gradient involved during synthesis procedure. Morphological study via HR-TEM suggests formation of spherical particles with narrow particle size distribution and well-defined grain boundaries. In-vitro anti-cancer activity of the samples was tested against three human carcinoma cell lines viz - Human Oral Squamous Cell Carcinoma (SCC-40), Human Melanoma Cell Line (SK-MEL-2) and Human Oral Squamous Cell Carcinoma (SCC-29B) cell lines, using Sulforhodamine B (SRB) assay. These results reveal that the cancer-cell selectivity of the ZnO samples was size dependent as different samples showed better activity to their corresponding cancer cell lines. NPs with smallest size have shown better anti-cancer activity and also good cell-kill. Therefore, it can be inferred that the samples prepared from C. *roseus*, A. *indica* and F. *religiosa* extract have excellent anti-cancer activity and also peculiar cell-selectivity. This combination, thus, may prove to be a potential anti-cancer agent for cancer therapy.

Acknowledgments

The authors would like to thank MHRD Government of India and MANIT Bhopal for providing scholarship to one of the authors (Vaibhav Koutu). Also, the authors would like to acknowledge Dr. O.P. Modi, Chief Scientist and Mr. Muhamad Shafeeq, Technical Assistant, Materials Characterization Laboratory, AMPRI Bhopal for X-ray diffraction characterization and Dr. Jyoti Kode (Officer In-charge, Anti-Cancer Drug Screening Facility (ACDSF), Advanced Centre for Treatment, Research & Education in Cancer (ACTREC), Tata Memorial Centre, Mumbai) for the in-*vitro* screening of the drugs for Anti-cancer activity analysis of the samples.

References

Ahmad, Z., Laughlin, T.F. and Kady, I.O. (2015), "Thymoquinone inhibits Escherichia coli ATP synthase and cell growth", *PloS one*, **10**(5), e0127802. https://doi.org/10.1371/journal.pone.0127802

Arakelova, E.R., Grigoryan, S.G., Arsenyan, F.G., Babayan, N.S., Grigoryan, R.M. and Sarkisyan, N.K. (2014), "In vitro and in vivo anticancer activity of nanosize zinc oxide composites of doxorubicin", *Int. J. Med. Heal. Pharm. Biomed. Eng.*, **8**, 33-38.

Ashrafi, A.A. (2011), In: *Encyclopedia of Semiconductor Nanotechnology*, (ed. Umar, A.), American Scientific Publishers, Chapter 10, p. 1.

Bisht, G. and Rayamajhi, S. (2016), "ZnO Nanoparticles: A promising anticancer agent", *Nanobiomedicine*, pp. 3-9. https://doi.org/10.5772/63437

DerMarderosian, A. and Beutler, J.A. (2012), *The review of natural products*: *the most complete source of natural product information*, Facts and Comparisons, St. Louis, MO, USA.

Dhamodarana, M. and Kavithab, S. (2015), "Anticancer Activity of Zinc Nanoparticles Made using Terpenoids from Aqueous Leaf Extract of Andrographis Paniculat", *Int. J. Pharmaceut. Sci. Nanotech.*, **8**(4), 3018-3023.

El-Sayed, I.H., Huang, X. and El-Sayed, M.A. (2005), "Surface plasmon resonance scattering and absorption of anti-EGFR antibody conjugated gold nanoparticles in cancer diagnostics: applications in oral cancer", *Nano Letters*, **5**(5), 829-834. https://doi.org/10.1021/nl050074e

Fang, J., Fan, H., Ma, Y., Wang, Z. and Chang, Q. (2015), "Surface defects control for ZnO nanorods synthesized by quenching and their anti-recombination in photocatalysis", *Appl. Surf. Sci.*, **332**, 47-54. https://doi.org/10.1016/j.apsusc.2015.01.139

Fiorillo, M., Verre, A.F., Iliut, M., Peiris-Pagés, M., Ozsvari, B.,

Gandara, R., Cappello, A.R., Sotgia, F., Vijayaraghavan, A. and Lisanti, M.P. (2015), "Graphene oxide selectively targets cancer stem cells, across multiple tumor types: implications for non-toxic cancer treatment, via "differentiation-based nano-therapy"", *Oncotarget*, **6**(6), 3553-3562. https://doi.org/10.18632/oncotarget.3348

Garcia-Contreras, R., Scougall-Vilchis, R.J., Contreras-Bulnes, R., Ando, Y., Kanda, Y., Hibino, Y., Nakajima, H. and Sakagami, H. (2014), "Effects of TiO2 nanoparticles on cytotoxic action of chemotherapeutic drugs against a human oral squamous cell carcinoma cell line", *in vivo*, **28**(2), 209-215.

Gurunathan, S., Han, J.W., Park, J.H., Kim, E., Choi, Y.J., Kwon, D.N. and Kim, J.H. (2015), "Reduced graphene oxide–silver nanoparticle nanocomposite: a potential anticancer nanotherapy", *Int. J. Nanomed.*, **10**, 6257-6276. https://doi.org/10.2147/IJN.S92449

Iwashita, K., Kobori, M., Yamaki, K. and Tsushida, T. (2000), "Flavonoids inhibit cell growth and induce apoptosis in B16 melanoma 4A5 cells", *Biosci. Biotechnol. Biochem.*, **64**(9), 1813-1820. https://doi.org/10.1271/bbb.64.1813

Kołodziejczak-Radzimska, A. and Jesionowski, T. (2014), "Zinc oxide–from synthesis to application: a review", *Materials*, **7**(4), 2833-2881.

Koutu, V. and Malik, M.M. (2017), "Method of biological synthesis of zinc oxide (ZnO) nanoparticles", Patent Application Publication India 201721923873A; (Filed on July 6, 2017, Published on September 22, 2017).

Koutu, V., Shastri, L. and Malik, M.M. (2016), "Effect of NaOH concentration on optical properties of zinc oxide nanoparticles", *Mater. Sci.-Poland*, **34**(4), 819-827. https://doi.org/10.1515/msp-2016-0119

Koutu, V., Shastri, L. and Malik, M.M. (2017), "Effect of temperature gradient on zinc oxide nano particles synthesized at low reaction temperatures", *Mater. Res. Express*, **4**(3), 035011. https://doi.org/10.1088/2053-1591/aa5855

Krishna, P.G., Ananthaswamy, P.P., Gadewar, M., Bora, U. and Mutta, N.B. (2016), "In vitro antibacterial and anticancer studies of ZnO nanoparticles prepared by sugar fueled combustion synthesis", *Adv. Mater. Lett.*, **8**(1), 24-29. https://doi.org/10.5185/amlett.2017.6424

Liu, M., Amini, A. and Ahmad, Z. (2017), "Safranal and its analogs inhibit Escherichia coli ATP synthase and cell growth", *Int. J. Biol. Macromolecule*, **95**, 145-152. https://doi.org/10.1016/j.ijbiomac.2016.11.038

Lucas, D.M., Still, P.C., Bueno-Perez, L., Grever, M.R. and Douglas Kinghorn, A. (2010), "Potential of plant-derived natural products in the treatment of leukemia and lymphoma", *Current Drug Targets*, **11**(7), 812-822. https://doi.org/10.2174/138945010791320809

Magnotta, M., Murata, J., Chen, J. and De Luca, V. (2006), "Identification of a low vindoline accumulating cultivar of Catharanthus roseus (L.) G. Don by alkaloid and enzymatic profiling", *Phytochemistry*, **67**(16), 1758-1764. https://doi.org/10.1016/j.phytochem.2006.05.018

Mittal, A.K., Chisti, Y. and Banerjee, U.C. (2013), "Synthesis of metallic nanoparticles using plant extracts", *Biotechnol. Adv.*, **31**(2), 346-356. https://doi.org/10.1016/j.biotechadv.2013.01.003

Mote, V.D., Purushotham, Y. and Dole, B.N. (2016), "Structural, morphological, physical and dielectric properties of Mn doped ZnO nanocrystals synthesized by sol–gel method", *Mater. Des.*, **96**, 99-105. https://doi.org/10.1016/j.matdes.2016.02.016

Nagajyothi, P.C., Muthuraman, P., Sreekanth, T.V.M., Kim, D.H. and Shim, J. (2017), "Green synthesis: in-vitro anticancer activity of copper oxide nanoparticles against human cervical carcinoma cells", *Arab. J. Chem.*, **10**(2), 215-225. https://doi.org/10.1016/j.arabjc.2016.01.011

Nam, K.C., Choi, K.H., Lee, K.D., Kim, J.H., Jung, J.S. and Park, B.J. (2016), "Particle size dependent photodynamic anticancer activity of hematoporphyrin-conjugated Fe 3 O 4 particles", *J. Nanomater.*, 1. https://doi.org/10.1155/2016/1278393

Namvar, F., Azizi, S., Rahman, H.S., Mohamad, R., Rasedee, A., Soltani, M. and Rahim, R.A. (2016), "Green synthesis, characterization, and anticancer activity of hyaluronan/zinc oxide nanocomposite", *OncoTargets Therapy*, **9**, 4549-4559. https://doi.org/10.2147/OTT.S95962

Pourrahimi, A.M., Liu, D., Ström, V., Hedenqvist, M.S., Olsson, R.T. and Gedde, U.W. (2015), "Heat treatment of ZnO nanoparticles: new methods to achieve high-purity nanoparticles for high-voltage applications", *J. Mater. Chem. A*, **3**(33), 17190-17200. https://doi.org/10.1039/C5TA03120F

Rasmussen, J.W., Martinez, E., Louka, P. and Wingett, D.G. (2010), "Zinc oxide nanoparticles for selective destruction of tumor cells and potential for drug delivery applications", *Expert Opinion Drug Delivery*, **7**(9), 1063-1077. https://doi.org/10.1517/17425247.2010.502560

Sankar, R., Maheswari, R., Karthik, S., Shivashangari, K.S. and Ravikumar, V. (2014), "Anticancer activity of Ficus religiosa engineered copper oxide nanoparticles", *Materials Science and Engineering: C*, **44**, 234-239. https://doi.org/10.1016/j.msec.2014.08.030

Tian, H., Fan, H., Li, M. and Ma, L. (2015), "Zeolitic imidazolate framework coated ZnO nanorods as molecular sieving to improve selectivity of formaldehyde gas sensor", *ACS SENSORS*, **1**(3), 243-250. https://doi.org/10.1021/acssensors.5b00236

Tian, H., Fan, H., Ma, J., Ma, L. and Dong, G. (2017), "Noble metal-free modified electrode of exfoliated graphitic carbon nitride/ZnO nanosheets for highly efficient hydrogen peroxide sensing", *Electrochimica Acta*, **247**, 787-794. https://doi.org/10.1016/j.electacta.2017.07.083

Xiao, F.X., Hung, S.F., Tao, H.B., Miao, J., Yang, H.B. and Liu, B. (2014), "Spatially branched hierarchical ZnO nanorod-TiO_2 nanotube array heterostructures for versatile photocatalytic and photo electrocatalytic applications: towards intimate integration of 1D-1D hybrid nanostructures", *Nanoscale*, **6**(24), 14950-14961.

Tang, L., Yang, X., Yin, Q., Cai, K., Wang, H., Chaudhury, I., Yao, C., Zhou, Q., Kwon, M., Hartman, J.A. and Dobrucki, I.T. (2014), "Investigating the optimal size of anticancer nanomedicine", *Proceedings of the National Academy of Sciences*, **111**(43), 15344-15349.

Tian, H., Fan, H., Ma, J., Liu, Z., Ma, L., Lei, S., Fang, J. and Long, C. (2018), "Pt-decorated zinc oxide nanorod arrays with graphitic carbon nitride nanosheets for highly efficient dual-functional gas sensing", *J. Hazard. Mater.*, **341**, 102-111. https://doi.org/10.1016/j.jhazmat.2017.07.056

Tiong, S., Looi, C., Hazni, H., Arya, A., Paydar, M., Wong, W., Cheah, S.C., Mustafa, M. and Awang, K. (2013), "Antidiabetic and antioxidant properties of alkaloids from Catharanthus roseus (L.) G. Don", *Molecules* 18, no. 8 (2013): 9770-9784.

Wang, C., Fan, H., Ren, X. and Fang, J. (2018), "Room temperature synthesis and enhanced photocatalytic property of CeO2/ZnO heterostructures", *Appl. Phys. A – Mater. Sci. Process.*, **124**(2), 99. https://doi.org/10.1007/s00339-017-1543-8

Zak, A.K., Majid, W.A., Abrishami, M.E. and Yousefi, R. (2011), "X-ray analysis of ZnO nanoparticles by Williamson–Hall and size–strain plot methods", *Solid State Sci.*, **13**(1), 251-256. https://doi.org/10.1016/j.solidstatesciences.2010.11.024